Phytoplankton detection study through hyperspectral signals in Patagonian Fjords

Pilar Aparicio-Rizzo[1, 2], Dagoberto Poblete-Caballero[1], Cristian Vera-Bastidas[1], Iván Pérez-Santos[1] and Daniel Varela[1]

[1]Centro i~mar, Universidad de Los Lagos, Puerto Montt, Chile

[2]Centro del Clima y la Resiliencia CR2, Santiago de Chile, Chile

5   *Correspondence to*: Daniel Varela (dvarela@ulagos.cl); Pilar Aparicio-Rizzo (papariciorizzo@gmail.com)

Abstract. Over recent decades, monitoring coastal areas has become a priority due to pressure from the human population. These areas constitute biodiversity enclaves where the increment in phytoplankton blooms has become a socio-ecological problem with severe impacts at global and regional scales. An important area they affect is the Patagonia Fjords, a complex and intricate coastal system strongly exposed to climate forcings and anthropogenic impacts with the aquaculture industry
10   (salmon and mussel farming) as the main source of income. Within this context, fast and accurate monitoring of phytoplankton in the area is crucial. In this study, we focus on using a new technology combining hyperspectral sensors and unmanned aerial vehicles (UAVs) to detect, identify, and differentiate phytoplankton species from optical data. Findings show differences not only between diatoms and dinoflagellates through the shape and magnitude of the spectral signal at 440, 470, 500, 520, 550, 570, and 580 nm but also at the genera level (*Rhizosolenia* sp., *Pseudo-nitzschia* sp., *Skeletonema* sp., *Chaetoceros* sp., and
15   *Leptocylindrus* sp.) and even species level like *Heterocapsa triquetra*. Chlorophyll-a concentration played a key role in reflectance spectra, showing high variability in the green-red bands (~ 500-750 nm) at low concentrations (< 2 µg L^{-1}), and even greater at the blue bands (~ 400-490 nm) under higher concentrations (> 4 µg L^{-1}). Although this work presents a step forward in using new tools and monitoring methodology of phytoplankton in complex coastal systems with a new identification route, more high-quality data from a wide range of ecosystems and environments is still necessary.

1 Introduction

Phytoplankton constitutes an essential group of organisms in aquatic ecosystems. As part of their essential role, they form the base of food webs, are key species in C and N biogeochemical cycles, and provide ecosystem services in the ocean (Legendre, 1990; Le Quéré et al., 2005). However, phytoplankton can also be harmful to the environment and humans. Intense phytoplankton blooms of many species have multiple negative impacts on coastal systems, including the suffocation of marine
25   organisms, negative aesthetic impacts on water quality, murky water sometimes containing floating dead organisms, and the unpleasant odours they produce. These negative impacts have significant consequences for local socio-economical activities (Berdalet et al., 2016; León-Muñoz et al., 2018; Díaz et al., 2019; Gobler, 2020). Furthermore, several phytoplankton species,

classified as HAB (> 100 known taxa) (Sournia, 1995), can produce toxins with severe consequences in aquatic systems, including water pollution and poisoning of marine organisms (shellfish, fish, mammals, birds, etc.), allowing the toxins to

30   enter the food chain, which can ultimately even affect humans.

Over recent decades, phytoplankton blooms have caused catastrophic events at both environmental and socio-economical levels worldwide (León-Muñoz et al., 2018; Trainer et al., 2020). An apparent global increase in the frequency and intensity of blooms is thought to be driven by climate change and/or anthropogenic eutrophication (Heisler et al., 2008; Anderson, 2012; Glibert, 2020; Gobler, 2020). Changes in the phytoplankton community are also expected due to changes in climate and coastal

35   systems, with consequences for the functioning of the biological carbon pump (Henson et al., 2021). These trends and the predicted demographic growth in coastal areas (Neumann et al., 2015; Merkens et al., 2016) require monitoring phytoplankton blooms to facilitate the essential tasks of forecasting, management and mitigation.

Traditionally, phytoplankton monitoring has been undertaken by collecting water samples at specific points and analysing those in the laboratory. This type of monitoring has several drawbacks, in that it is time consuming, expensive, and labour

40   intensive, making large-scale monitoring over a short period impractical. As a result, the monitoring of phytoplankton by remote sensing using satellites was implemented. Monitoring of phytoplankton in surface waters by satellites has been widely used for decades due to their broad spatial coverage and high temporal resolution (Alvain et al., 2008; Brewin et al., 2011; Li et al., 2021). Identification of phytoplankton by remote sensing is mainly based on how the species attributes affect the absorption/reflectance of the electromagnetic spectrum. The optical properties of phytoplankton, such as pigment

45   concentration (algae colour), size, and morphology, affect the reflectance signal, allowing different groups to be distinguished (Alvain et al., 2008; Brewin et al., 2011; Moisan et al., 2017). Spectral bands located in the blue, green, and red to near-infrared areas of the spectrum can be used to detect algal blooms (Mao et al., 2010; Brewin et al., 2011; Shen et al., 2012; Gernez et al., 2023). Differences in the major absorption and/or reflectance peaks have been related to the colour of the algae and chlorophyll type and concentration (Mao et al., 2010; Tao et al., 2013; Moisan et al., 2017). In the green band, a peak around

50   570-580 nm has been associated with Bacillariophyta and Haptophyta (brown algae); meanwhile, Chlorophyta (green algae), known to contain chlorophyll-b, display peaks around 540 nm due to their green colour (Jeffrey and Vesk, 1997; Gitelson et al., 1999; Mao et al., 2010). Although satellite technology has provided important advances in large-scale phytoplankton monitoring, it has limitations. This technology has been useful for detecting and differentiating between the main phytoplankton groups and even red tides (Hu et al., 2005; Shen et al., 2012; Zhao and Ghedira, 2014; Gernez et al., 2023).

55   However, the spatial-temporal resolutions themselves, the satellite orbit (revisit cycle), the limited surface-subsurface signal capture or the restricted number of reflectance bands are considered the main obstacles to the discrimination of the dominant bloom-forming species and the identification of the algae (Muller-Krager et al., 2018; Schaeffer and Myer, 2020).

Moreover, phytoplankton monitoring is complex in regions with high environmental heterogeneity at different scales. For instance, in sub-polar coastal areas, like the Patagonian Fjords, satellite information availability is limited for part of the year

60   due to high cloudiness and complex coastal morphology (i.e., fjords and channels). Across this coastal area, there is a two-

layer water circulation pattern (Valle-Levinson, 2010; Castillo et al., 2016), consisting of a surface layer fed by continental freshwater (Estuarine Water-EW) from rivers, high rainfall and glacial meltwater, flowing from the continent, and a subsurface layer of salty, nutrient-rich Sub-Antarctic Waters (SAAW) coming from the western Pacific Ocean (Dávila et al., 2002; Pérez-Santos et al., 2014; Linford et al., 2024). This current circulation results in marked vertical and horizontal gradients with

65 significant meridional and zonal changes in temperature, salinity, stratification, and suspended matter (CDOM & TSM) (Silva and Vargas, 2014; Torres et al., 2014; González et al., 2019; Saldías et al., 2019; Linford et al., 2024). Consequently, this environmental variability highly influences phytoplankton distribution, abundance, and HAB occurrence (Alves-de-Souza et al., 2008; Jacob et al., 2014; León-Muñoz et al., 2018; Cuevas et al., 2019). At local scales, physical processes like stratification, triggered by both river discharge and seasonal solar heating, and biogeochemical water characteristics, including

70 suspended particulate matter (CDOM and TSM) and phytoplankton concentration, significantly influence the water's optical properties (Simis et al., 2017; Adhikari et al., 2023). Coastal and estuarine waters are considered optically complex due to their high charge and temporal (from daily to seasonal) variability in both biological (phytoplankton) and non-biological (CDOM & TSM) suspended particles that impact directly at optical signal affecting the water transmission of irradiance (Simis et al., 2017; Adhikari et al., 2023).

75 The accurate observation of phytoplankton in coastal areas where phytoplankton population characteristics can change rapidly over short time scales (hours to days) and at small spatial scales (< 100 m) represents a significant challenge. This observation is important in the Patagonian Fjords, which hosts one of the largest aquaculture industries globally (salmon and shellfish). These industrial activities have suffered recurrent Harmful Algal Blooms (HAB), experiencing significant damage over recent decades (León-Muñoz et al., 2018; Díaz et al., 2019), with remarkable social, economic and ecosystemic impacts (Soto et al.,

80 2019; Ugarte et al., 2022). Thus, developing and implementing an effective phytoplankton monitoring regime with high accuracy and resolution is essential. However, this is a tough task due to the complexity and unknown aspects of phytoplankton bloom dynamics, together with the broad species diversity involved and the geographical (complex topography) and climate (cloudy hyper-humid) heterogeneity (Garreaud et al., 2013).

Monitoring at the required spatial and temporal resolution can now be achieved due to advances in technology, including

85 unmanned aerial vehicles (UAVs) equipped with sensitive instruments, which have recently become more widely used as platforms in marine monitoring (Kislik et al., 2018; Kimura et al., 2019; McEliece et al., 2020; Hong et al., 2021). Specifically, the use of multi- and hyperspectral cameras that capture in situ reflectance signals at low altitudes (< 200 m) through the visible to near-infrared regions of the spectrum (~ 400-1000 nm) out-performing multispectral cameras and satellites (Moses et al., 2012; Olivetti et al., 2023). Identification of phytoplankton species by hyperspectral images provides a new tool for monitoring

90 the temporal and spatial variation at the local scale in coastal ecosystems in situ. This optical technology has the potential for monitoring phytoplankton and detecting HAB in coastal environments due to its continuous spectrum bands, which allow for an accurate phytoplankton characterisation through reflectance (Van der Merwe and Price, 2015; Wu et al., 2019; Olivetti et al., 2023). Recent studies have illustrated the usefulness of this technology for detecting phytoplankton blooms through the

accumulations of algae (Szekielda et al., 2007) or the differences in reflectance spectra between recurrent and non-recurrent

95   blooms areas with changes in the green (~ 545-575 nm) and red bands (~ 650-700 nm), respectively (Min et al., 2021).

In the present study, we explore the advantages and disadvantages that a hyperspectral camera, coupled with a UAV, offers in detecting phytoplankton from reflectance (R(λ)) at complex coastal waters in remote areas. The main objective was the characterisation of the reflectance spectra of different phytoplankton assemblages, either harmful or non-harmful, dominated by a single species. By analysing differences in the magnitude and shape of the spectral signal, we seek to distinguish distinct

100   phytoplankton groups.

2 Materials and methods

2.1 Study area

The study area is located within one of the 3 main fjords' regions worldwide at north Patagonia (~ 41.45-42.75° S) in southern Chile (Fig. 1), where most of the national aquaculture activities (salmon, blue mussels, and macroalgae) are found (> 90 %)

105   (Soto et al., 2019).
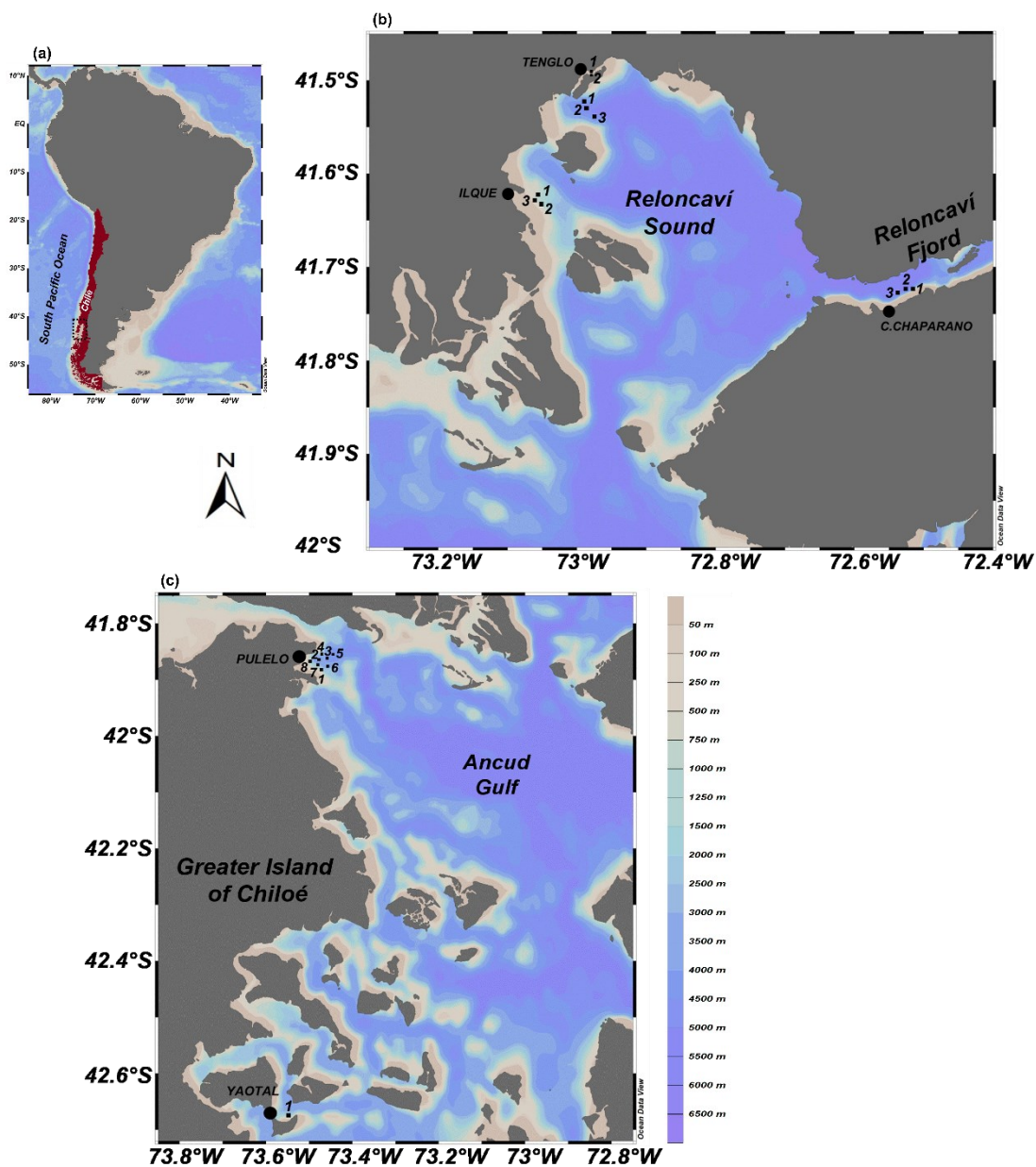
Figure 1: (a) Study area and sampling locations at (b) Reloncaví and (c) Greater Island of Chiloé in the northern Patagonian Fjords (~ 41.45-42.75° S).

110   Across this complex coastal system, freshwater inputs from rivers, precipitation, groundwater, and glacial melting generate an estuarine circulation pattern (Dávila et al., 2002; Valle-Levinson, 2010; Castillo et al., 2016), with considerable influence over biogeochemical processes and physical oceanography. The freshwater inputs generate stratification conditions that strongly

influence bio-optical water properties and support a diatoms-dominated phytoplankton community (Iriarte et al., 2007; Silva et al., 2011; González et al., 2019).

2.2 Field sampling

This study implemented an integrated field sampling strategy from January to May 2023 (austral summer-autumn) in the coastal system to acquire in situ hyperspectral images and oceanographic data for temperature, salinity, and phytoplankton. Specific sectors were selected for the in situ sampling across the study area (Fig. 1) based on a set of criteria, including historical physical-chemical characteristics (temperature, salinity, and turbidity), local circulation, HAB occurrence, and proximity to aquaculture installations (Table 1) (Silva et al., 2011; Soto et al., 2019; Soto et al., 2021).

Table 1: Characteristics of in situ sampling sectors.

Location	Latitude	Longitude	Characteristics and criteria for selecting the sampling area
Ilque (I)	-41.621/-41.630	-73.059/-73.064	Semi-enclosed circulation area Clear-Turbid waters Strong marine influence HAB moderate risk
Isla Tenglo (I)	-41.524/-41.538	-72.969/-72.991	Open circulation area Clear waters Strong marine influence HAB moderate risk
Canal Tenglo (CT)	-41.495/-41.498	-72.9836/-72.9837	Enclosed circulation area Turbid waters Marine influence HAB moderate risk
C. Chaparano (C)	-41.724/-41.727	-72.519/-72.536	Intense mussel farm activity Enclosed circulation area Turbid waters Freshwater influence HAB high risk Historical HAB occurrence
Pulelo (P)	-41.855/-41.873	-73.466/-73.480	Intense salmon culture activity Open circulation area Clear waters Strong marine influence HAB medium risk
Yaotal (Y)	-42.672	-73.548	Intense salmon culture activity Open circulation area Clear waters Strong marine influence HAB medium risk

Six locations were defined across the area using these criteria: Ilque (I), Isla Tenglo (T), and Canal Tenglo (CT) within the Reloncaví sound coastal system, Caleta Chaparano (C) in Reloncaví fjord, and two sampling points along the coast of the Isla Grande de Chiloé, Pulelo (P) and Yaotal (Y) (Table1, Fig. 1b & c). At these monitoring locations, sampling transects of 3 or 4 stations were carried out depending on topography and UAV flight autonomy.

The field sampling was carried out during daylight (~ 10.30-16.00 h) under safe and optimal weather conditions. Although meteorological conditions varied between sunny and cloudy days, all sampling transects were conducted with conditions of no rain, low wind speed (< 15 m s⁻¹), and calm surface waters (waves < 1 m).

Water samples for oceanographic monitoring were collected simultaneously with the optical data at each station. The geo-location (latitude/longitude) was sent from the vessel equipment to the UAV technician on shore to coordinate the water sampling with the aerial observations. The autonomous flights were configured using the DJI Pilot 2 drone software for an altitude of 100 m above the sea surface and a flight speed of ~ 1-2 m s⁻¹ according to in situ solar radiation to obtain images of an area of 2500 m² around the oceanographic sampling points.

As phytoplankton is commonly distributed within the first ~ 20-30 m of the water column, two sampling depths were established: the first at the surface (~ 1.5 m) and the second based on water transparency. Temperature, salinity and Chlorophyll-a (Chl-a) were determined using a RBRconcerto³ and AML-Oceanographic Metric XL CTDs, and transparency by a Secchi disk. Water samples were collected using a Niskin bottle at the surface and Secchi depths and stored in opaque plastic bottles to be analysed at the laboratory for both phytoplankton in situ total biomass (Chl-a) and phytoplankton abundance and taxonomy. Discrete water samples collected for analyses of phytoplankton abundance and taxonomy were fixed with Lugol's iodine solution (1 %).

2.3 Phytoplankton analysis

Phytoplankton total biomass (Chl-a) and species abundance were estimated in the microphytoplankton range (~ 20-200 μm) at the laboratory. The phytoplankton identification and cell counts were made following the Utermöhl method (Utermöhl, 1958), i.e. 10 mL of fixed water sample was settled from day to day and then observed using an inverted light microscope (Olympus CKX-41). Taxonomic identification was made to the lowest level possible (genus or species) (Mardones and Clément, 2016; Lincoqueo, 2019).

For total biomass analysis (Chl-a), 2 L of water was filtered using a vacuum filtration system and Whatman glass-fiber filters of 0.7 μm pore size. The filters were kept in the dark and at - 80° C for later fluorometry analysis.

2.4 UAV system, reflectance measurement and hyperspectral image

The UAV used in this study was a DJI Matrice 300 RTK drone with the capacity to support a maximum weight of ~ 9 kg and a flight autonomy of approximately 30 minutes (Fig. 2a). A hyperspectral camera Resonon Pika L model was coupled to the drone by a custom made 3D printed carbon fibre gimbal (Fig. 2b). In addition, a minicomputer Intel NUC was carried by the drone attached using a custom 3D printed mount, including batteries (Fig. 2b).
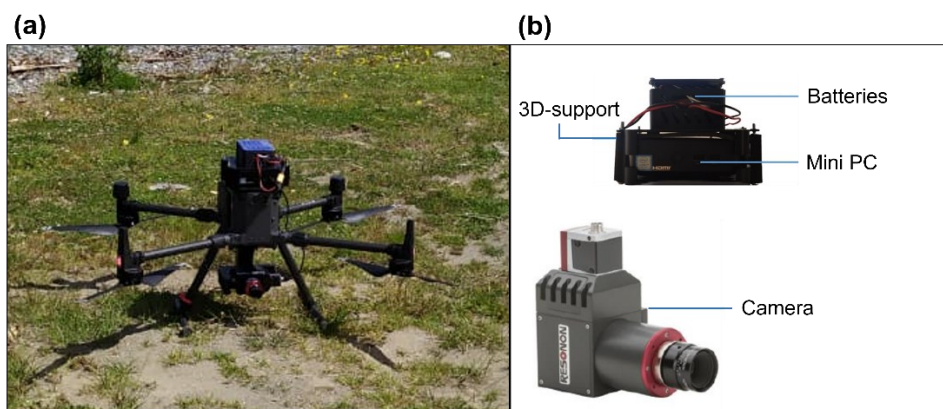
Figure 2: UAV system: (a) DJI Matrice 300 RTK drone, and (b) Resonon Pika L hyperspectral camera, and the 3D printed mount with the batteries and minicomputer Intel NUC.

160

The camera captures 236 spectral bands covering a spectrum range from ~ 400 to 900 nm with a spectral resolution of approximately ~ 2.1 nm. A Flame S spectrometer was used to record the light conditions (solar radiation) during the flight in the same spectral bands as those captured by the hyperspectral camera.

A laptop connected via a cellular connection or a WLAN network to the minicomputer was used to operate the camera and
165 record reflectance data. In remote areas where connectivity was not available, communication between computers was established by an Access Point Ubiquiti Loco M5 through a local wireless network.

2.5 Data processing

Before the data analyses, a pre-selection was performed, removing all the samples with several co-occurring phytoplankton genera (> 3) from the final dataset. Only stations where one or a maximum of two genera dominated the community by > 80
170 % of abundance were considered for the reflectance fingerprint analysis and the differentiation among the spectral signals. Several phases were involved in processing the raw image data captured by the hyperspectral sensor using the Spectronon Pro software. First, solar radiation raw data were processed to obtain solar reflectance ($R(\lambda)$). To reduce the signal noise and obtain a clean spectral signal a Savitzky-Golay double filter was applied to smooth the spectral curve without altering its properties (Ruffin and King, 1999; Gallagher, 2020). In the following step, pixel cleaning by an adapted NDWI index was undertaken,
175 masking those pixels that did not correspond to water and those saturated due to solar radiation angle incidence (Xie et al., 2014). Finally, reflectance raw data were averaged and normalised by the min-max technique, obtaining a reflectance value at each band to emphasise the shape singularities of each spectrum.

For analysing and comparing the spectral signals of the different phytoplankton species, the reflectance $R(\lambda)$ values were used at a spectral resolution of ~ 2.1 nm approx., and the wavelength bands were limited to the visible and near-infrared light
180 between 400 and 750 nm.

 A hierarchical cluster analysis (HCA) was made to explore the changes in R(λ) under different genera domains. A resemblance matrix based on the hyperspectral normalised R(λ) was generated using the nearest neighbour single linkage algorithm and the cosine index as a distance measure for calculating the similarity among spectral signals.

Differentiation among spectral signals for the stations under the same phytoplankton genera domain was analysed using the
185 non-parametric Kolmogorov-Smirnov test. In addition, to assess the influence of pigment concentration at spectral signals, a statistical analysis was applied to determine the differences among low ($< 2\ \mu g\ L^{-1}$), moderate ($> 4\ \mu g\ L^{-1}$) and high ($> 8\ \mu g\ L^{-1}$) Chl-*a* concentrations.

Oceanographic variables across the study area were characterised at a seasonal scale and in-depth using a principal component analysis (PCA) to produce an ordination of sampling stations, followed by a permutational analysis of variance (One-way
190 PERMANOVA) to determine the differences between stations. Before the analysis, data were homogenised (log-transformed) and normalised to better approximate multivariate normality.

Data were visualised and processed using Ocean Data View (ODV) (Schlitzer, 2023), which applied DIVA gridding interpolation (Troupin et al., 2012), PRIMER 7 (Clarke and Gorley, 2015), and PAST 4.06 software (Hammer et al., 2001).

3 Results

195 ### 3.1 Oceanographic Conditions

The temperature profiles generally displayed surface warming, especially in summer, with a clear development of thermal stratification conditions (Fig. 3a).
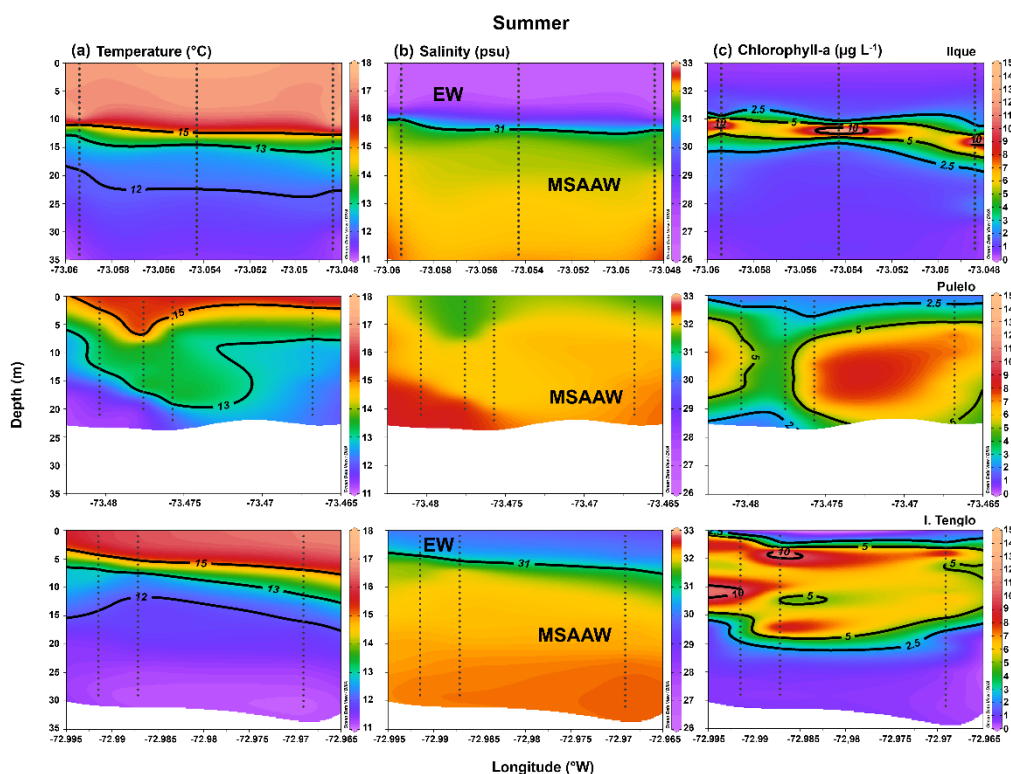
Figure 3: Oceanographic conditions of (a) Temperature, (b) Salinity, and (c) Chlorophyll-a at the sampling locations during
summer. EW (Estuarine Water), MSAAW (Modified Sub-Antarctic Water).

Temperatures in the autumn were generally lower (a difference of ± 2.2-5.7° C) with weaker depth gradients, except for
Chaparano in the Reloncaví fjord (Fig. 4a).
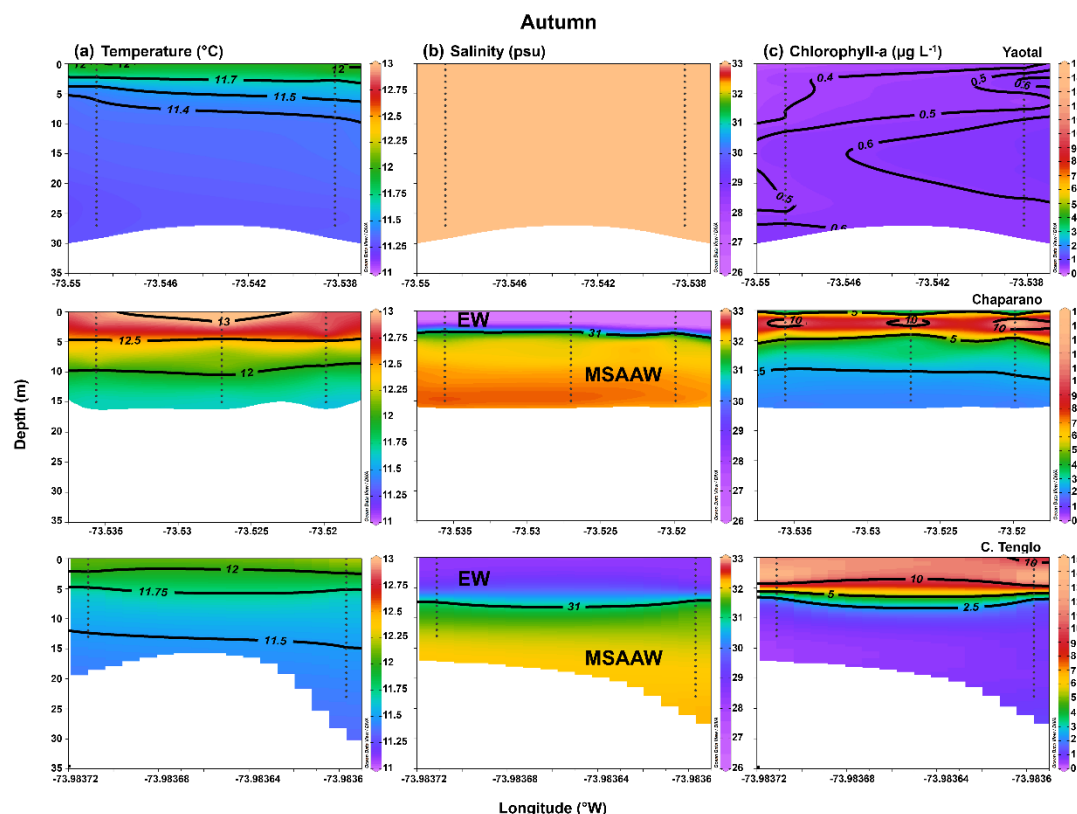
Figure 4: Oceanographic conditions of (a) Temperature, (b) Salinity, and (c) Chlorophyll-a at the sampling locations during autumn. EW (Estuarine Water), MSAAW (Modified Sub-Antarctic Water).

Freshwater input clearly influenced the salinity observed around the Reloncaví sound and within the fjord (Fig. 3b and 4b), with the lowest salinity values at Chaparano (Table 2). On the other hand, an influence of oceanic water was detected, with the highest salinity, at Isla Grande de Chiloé, where estuarine water (EW) was not detected (Fig. 3b and 4b).

Table 2: Oceanographic conditions of temperature (T), salinity (S), and chlorophyll-a (Chl-*a*) at the sampling locations. Mean, standard deviation (SD) and range (maximum-minimum).

Sampling Location	Station	Date	Mean T±SD (°C)	Mean S±SD	Mean Chl-*a*±SD (µg L⁻¹)	Range T (max.-min.) (°C)	Range S (max.-min.)	Range Chl-*a* (max.-min.) (µg L⁻¹)
Ilque	I1/I2	05/01/2023	17.34±0.17	26.977±0.08	0.799±0.35	17.48-17.12	27.075-26.883	1.043-0.555
Pulelo	P1/P2/P3/P4	18/01/2023	14.94±0.60	31.696±0.16	2.916±1.01	14.02-15.51	31.905-31.482	4.788-2.020
Isla Tenglo	T1/T2/T3	26/01/2023	16±0.49	30.161±0.35	5.926±4.51	15.22-16.64	30.697-29.692	12.214-1.582
Ilque	I3	31/03/2023	12.36±0.25	31.956±0.03	1.551±0.82	12.18-12.54	31.934-31.977	0.974-2.127
Yaotal	Y1	12/04/2023	11.66±0.45	33.286±0.01	0.443±0.16	11.35-11.98	33.276-33.296	0.326-0.559

| Chaparano | C1/C2/C3 | 14/04/2023 | 12.76±0.20 | 26.388±5.69 | 4.576±1.14 | 13.01-12.47 | 31.727-20.053 | 6.099-3.206 |
| Canal Tenglo | CT1/CT2 | 09/05/2023 | 11.99±0.20 | 28.788±0.28 | 10.163±1.41 | 12.21-11.79 | 29.07-28.55 | 11.47-8.54 |

In the summer, Chl-*a* concentrations were highest around the transitional depth between the estuarine and modified sub-
215 Antarctic water masses (Fig. 3c). Meanwhile, in autumn, the highest values were detected in the low salinity surface waters
(EW) (Fig. 4c), with a minimum in Chl-*a* at Yaotal under a homogeneous water column (Fig. 4c, Table 2) and the maximum
at Canal Tenglo associated with a phytoplankton bloom event (Fig. 4c). Across the sampling locations, the highest values (>
4 µg L^{-1}) and largest ranges were observed in enclosed waters, i.e., Chaparano and both Canal Tenglo and Isla Tenglo (Fig.
1b, Table 2).

220 The analysis of the oceanographic variables' spatial patterns (temperature, salinity, and Chl-*a*) indicates that 74 % of
oceanographic variability is explained by the first two components (Fig. 5). For the first component (PC1), the highest
eigenvector was exhibited by Chl-*a* (- 0.67) followed by temperature (0.62), with both variables significantly associated with
PC1 scores (p < 0.01). Meanwhile, salinity was significantly correlated with PC2 scores (p < 0.01), with the relevant
eigenvector (- 0.89) in the second component (PC2).
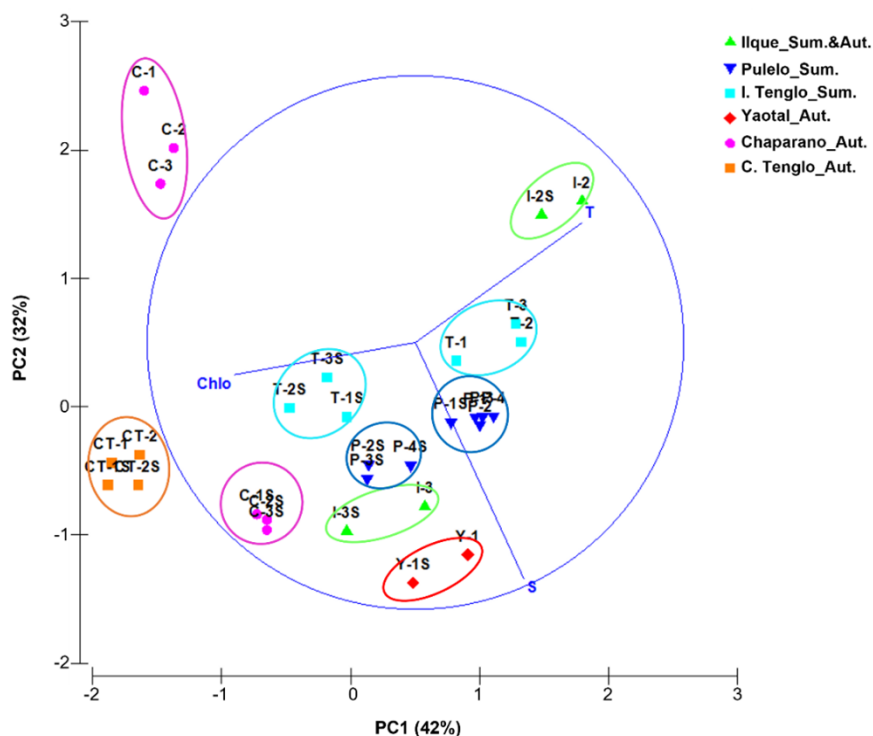
225

Figure 5: Spatial ordination diagram of sampling locations based on oceanographic conditions (blue vectors T, S, Chlo) at Surface and Secchi depths (S), observed during Summer (Sum.) and Autumn (Aut.). T= temperature, S= salinity, and Chlo= chlorophyll-a.

This analysis indicates that the summer samples at Ilque (I-2), Pulelo (P) and Isla Tenglo (T) were mainly influenced by temperature and Chl-*a* (Fig. 5). Whereas autumn samples were influenced by Chl-*a* and salinity (Fig. 5). Chaparano I and Canal Tenglo (CT) were mainly influenced by Chl-*a*, but Yaotal (Y) and Ilque (I-3) by salinity (Fig. 5).

Significant differences in oceanographic conditions were registered between seasons (F= 8.18, p < 0.01), but not between depths (F= 2.2, p > 0.05). However, in summer, differences were observed in Chl-*a* and temperature between surface and Sechii depth at both Pulelo and Isla Tenglo (Fig. 5). While, in autumn, there was a pronounced difference in salinity with depth at Chaparano (Fig. 5).

3.2 Phytoplankton and spectral signals

Although the phytoplankton community was typical of the summer-autumn diatoms assemblage described for the area, the community composition changed between seasons, with an increase in diversity and a decrease in dominance together with a slight increase in richness in the autumn, with the exception of Canal Tenglo (Fig. 6, Table S1).
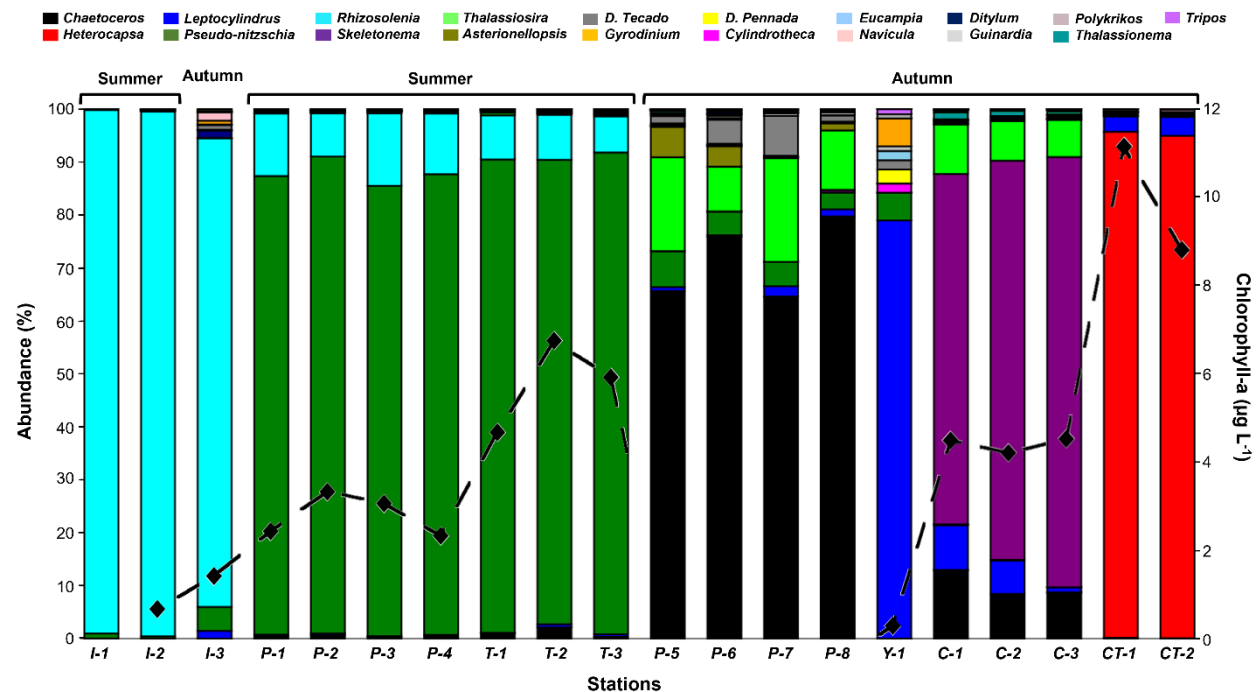
Figure 6: Microphytoplankton community composition (histogram) and total biomass (black line) during summer and autumn at sampling locations. Each colour represents a genre of the community. Code locations: I= Ilque, P= Pulelo, T= Isla Tenglo, Y= Yaotal, C= Chaparano, and CT= Canal Tenglo.

Even though only a bloom of microalgae *Heterocapsa triquetra* was detected during the study period, composition analysis
245 showed a clear mono-genus domain (> 80 % abundance) of *Rhizosolenia* sp. at Ilque and *Pseudo-nitzschia* sp. at Pulelo and
Isla Tenglo in the summer (Fig. 6). On the other hand, in autumn a combination of two genera was needed to reach 80 %
abundance at Chaparano, Yaotal and Pulelo (Fig. 6).

Although the reflectance spectrums, under a diatom genus domain, displayed quite similar patterns across the blue and green
bands (~ 400-565 nm), differences in the shape of the curve and the reflectance values were observed, even between sample
250 stations at the same location (Fig. 7 and 8). During summer, samples at Ilque, dominated by *Rhizosolenia* sp., displayed
significant differences in the spectral signal ($p < 0.01$) between stations in both the blue (~ 400-490 nm) and green to near
infra-red bands (~ 500-750 nm) (Figure 7a).
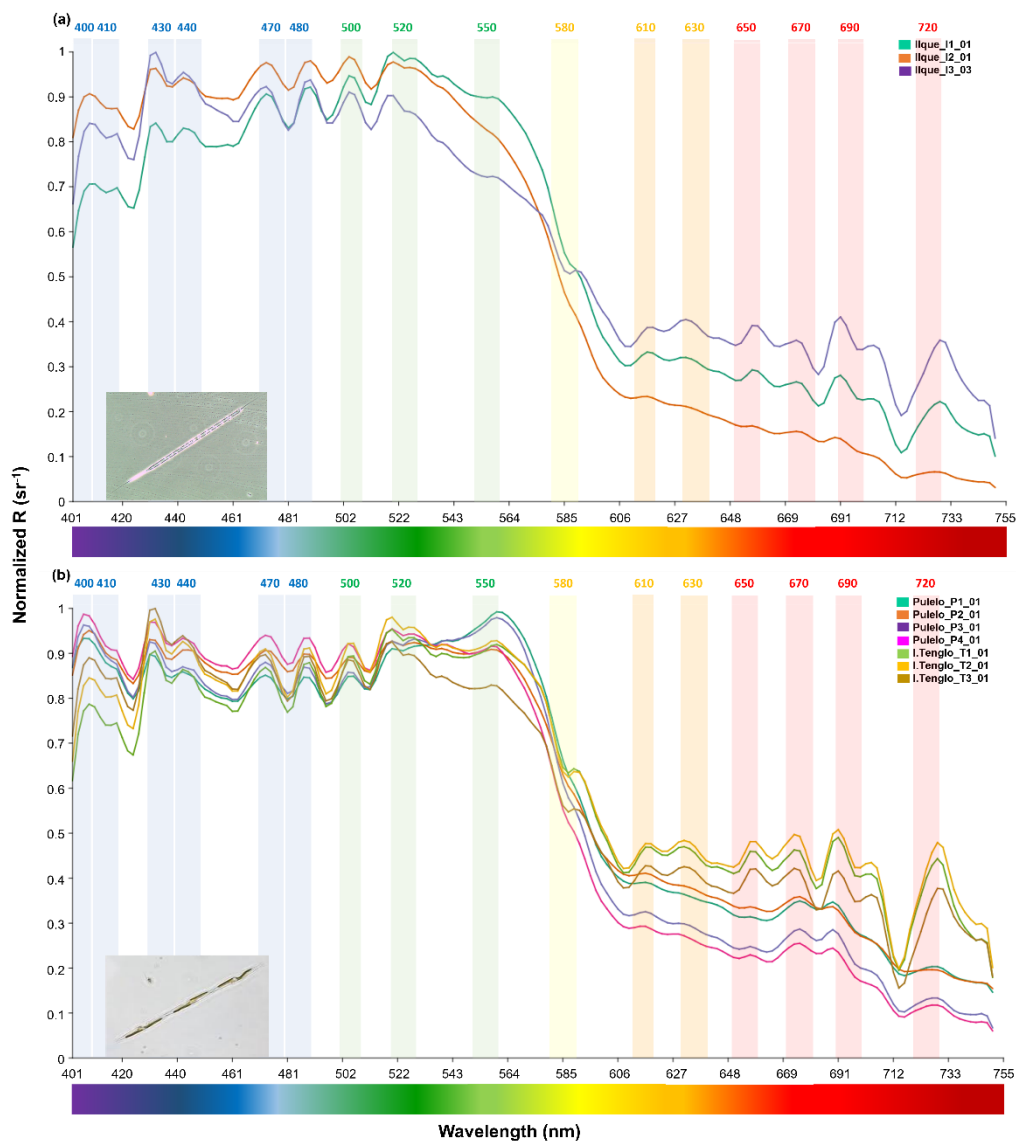
Figure 7: Diatoms spectral signals: (a) *Rhizosolenia* **sp. at Ilque (aqua green, orange and purple), and (b)** *Pseudo-nitzschia* **sp. at Pulelo (aqua green, orange, purple and pink) and Isla Tenglo (jasmine green, yellow and brown) in north Patagonia (~ 41.45°-42.75° S).**

Similarly, under *Pseudo-nitzschia* sp. domain, significant spectral differences ($p < 0.01$) were detected at Pulelo. In the blue bands (~ 400-490 nm), similar signals at stations 1 and 3 differ from stations 2 and 4 (Fig. 7b). Meanwhile, from green to the near infra-red bands (~ 500-750 nm), stations 1 and 2 differed significantly in the spectral signal at stations 3 and 4 (Fig. 7b). On the other hand, at Isla Tenglo, only station 3 displayed a spectral signal significantly different in the green to the near infra-red bands (~ 500-750 nm) (Fig. 7b).

Generally, the analysis displayed a more homogeneous reflectance signal from March to April (autumn) samples (Fig. 8). At
265 Pulelo, similar spectral signals were detected, except for station 8 (Fig. 8a, pink), in the green to the near infra-red bands (~
500-750 nm) (Fig. 8a). Also, only station 2 at Chaparano (Fig. 8b, orange) displayed a statistically different (p < 0.01) signal
in the blue band (~ 400-490 nm) (Fig. 8b).
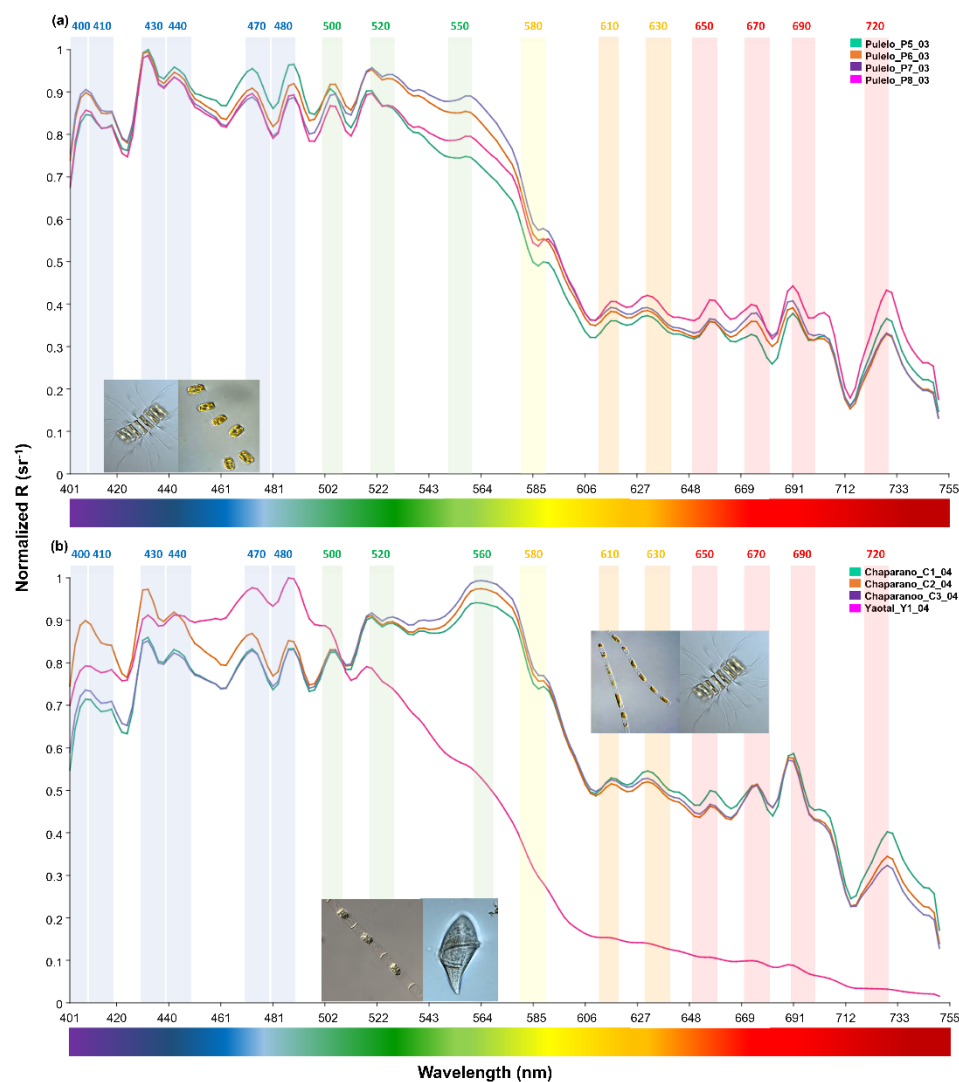
270 **Figure 8: Diatoms spectral signals: (a) *Chaetoceros* sp. & *Thalassiosira* sp. at Pulelo (aqua green, orange, purple and pink), and (b)**
***Skeletonema* sp. & *Chaetoceros* sp. at Chaparano (aqua green, orange and purple), and *Leptocylindrus* sp. & *Gyrodinium* sp. at Yaotal**
(pink) in north Patagonia (~ 41.45°-42.75° S).

A comparison between the bands indicated that all samples under diatoms genera domain displayed a similar pattern in the blue bands (~ 400-490 nm), except for *Leptocylindrus* sp. at Yaotal, with the highest R(λ) (> 0.9 sr⁻¹) registered at 470-480 nm (Fig. 8b). In the green bands (~ 500-565 nm), where chlorophyll pigments reflect light, generally high values of reflectance (> 0.9 sr⁻¹) were recorded, but also a higher variability in both shape and R(λ) values (Fig. 7 and 8). In fact, at Ilque, where *Rhizosolenia* sp. dominated, the reflectance exhibited an acute downward slope between the green and yellow bands (~ 550-610 nm) (Fig. 7a), where the absorption peaks of accessory pigments such as phycoerythrin and phycocyanin are usually detected. A similar slope was observed at Pulelo and Isla Tenglo under *Pseudo-nitzschia* sp. domain (Fig. 7b). While, at Chaparano, this slope was less pronounced (Fig. 8b).

Finally, the spectral reflectance from all diatom genera displayed a declining slope in the red to near-infra-red bands (~ 650-740 nm), where another peak in chlorophyll reflectance is typically described. In this area of the spectrum, two main peaks were observed between ~ 680-720 nm and an acute decline at ~ 714 nm (Fig. 7 and 8). A Strong variability was registered among genera in this area of the spectrum, with the highest values detected at Chaparano for the *Skeletonema* and *Chaetoceros* sp. assemblage (Fig. 8b).

Furthermore, important differences were observed in the spectra between diatoms and dinoflagellates. The spectral signal of dinoflagellates was captured only once, under a bloom of the species *Heterocapsa triquetra*. The spectrum shape of this species displayed a completely different pattern compared to those of diatom genera. In the *Heterocapsa triquetra* spectral signal, a clear increase in the R(λ) from the blue to green bands (~ 400-565 nm) can be observed (Fig. 9).
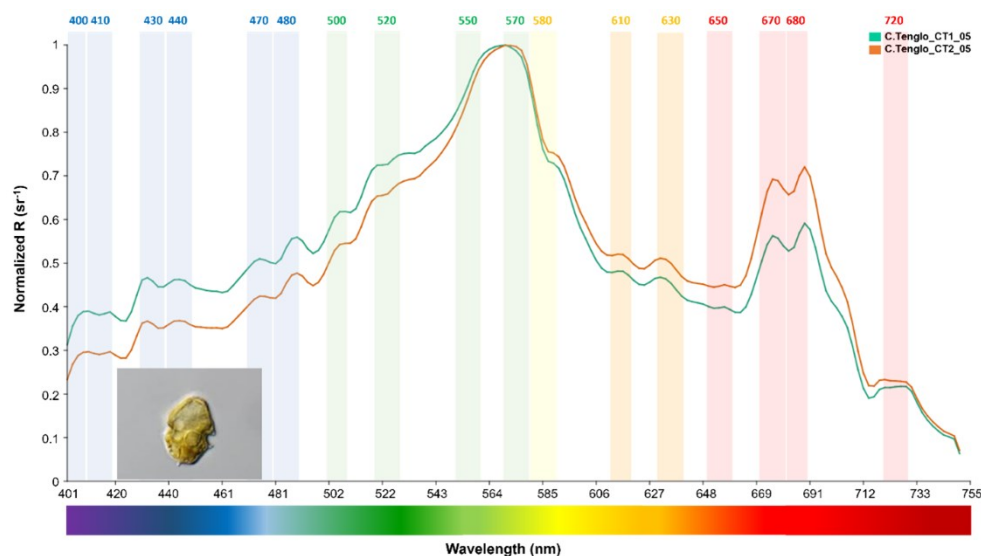
Figure 9: Dinoflagellate *Heterocapsa triquetra* spectral signal at Canal Tenglo (aqua green-Sta.1, orange-Sta.2) in north Patagonia (~ 41.45°-44.75° S).

R(λ) values were two or three times lower than for diatoms in the blue bands (~ 400-490 nm), with differences between station signals (Fig. 7, 8 and 9). The main peak of R(λ) was at 570 nm in the yellow-green area (Fig. 9). Differences between

295   dinoflagellates and diatoms were also registered in the red to near infra-red bands (~ 650-740 nm) with a distinctive signal of two R(λ) peaks at 670 and 680 nm (> 0.55 sr^{-1}), together with a plateau structure at 720 nm (Fig. 7, 8 and 9).

In summary, differences between groups were detected through the shape (Fig. 7, 8 and 9), the peaks observed at 440, 470, 500, 520, 550, 570, and 580 nm, and the variations in the magnitude displayed in the blue-green (~ 400-565 nm) and red to near infra-red bands (~ 650-740 nm) (Fig. 7, 8 and 9). As a result, the cluster analysis grouped spectra corresponding to stations

300   under the same dominant groups and genera closer (Fig. 10).
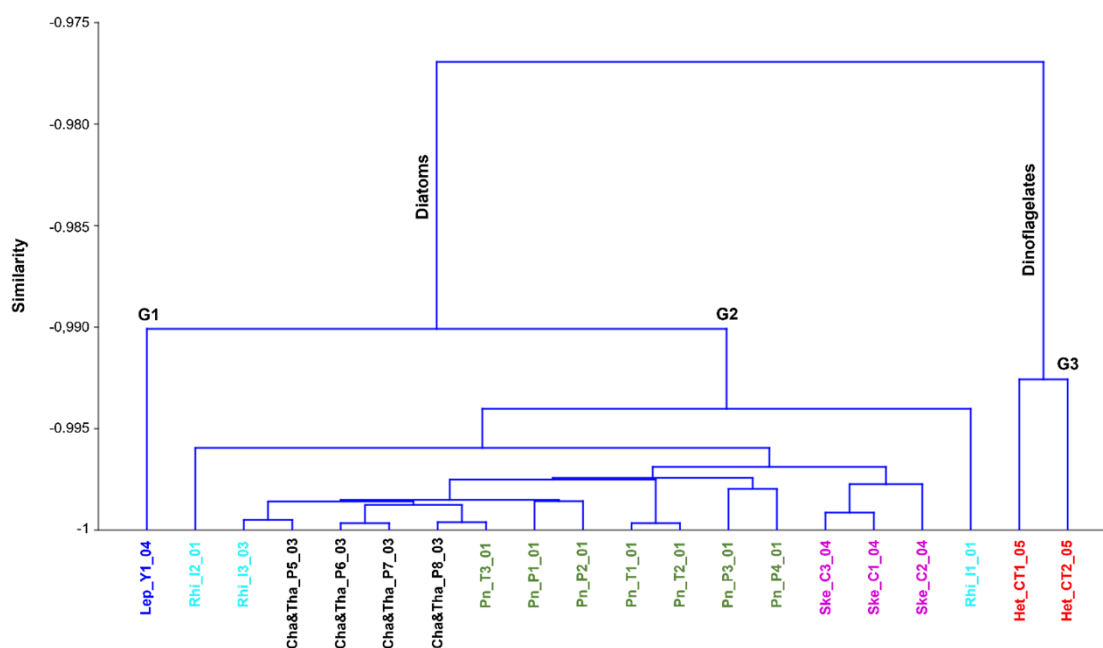
Figure 10: Dendrogram of microphytoplankton hyperspectral normalised R(λ) signals classified by the dominant genera. Colours identify different genus and sampling locations: *Leptocylindrus* **sp. in Yaotal (blue),** *Rhizosolenia* **sp. in Ilque (cyan),** *Chaetoceros* **sp. &** *Thalassiosira* **sp. in Pulelo (black),** *Pseudo-nitzschia* **sp. in Pulelo & Isla Tenglo (green),** *Skeletonema* **sp. in Chaparano (violet) and**
305   *Heterocapsa triquetra* **in Canal Tenglo (red).**

Although similarity values were high, two main divisions were identified: one grouping locations dominated by diatoms and another dominated by the dinoflagellate *Heterocapsa triquetra* (Canal Tenglo) (Fig. 10).

Within the diatoms, 2 groups can be described: a first group (G-1) at Yaotal during the autumn, dominated by *Leptocylindrus* sp. (78.95 %), with the dinoflagellate *Gyrodinium* sp. (5.26 %) as the secondary genus. The second (G-2) grouped the rest of
310   the locations dominated by diatoms (Fig. 10). Within G-2, all samples were grouped by the dominant genus except Ilque (Fig. 10).

Nevertheless, the dendrogram grouped locations based on not only the dominant genera but also under similar oceanographic conditions (Fig. 10). Thus, on the left side of the cluster, Yaotal (blue) and Ilque (cyan) were associated with changes in salinity during the autumn season and characterised by low Chl-*a* values. On the opposite side (right), Canal Tenglo (red) and

315   Chaparano (violet) locations were characterised by the register of high Chl-*a* values.

Therefore, reflectance spectra displayed variability under different chlorophyll-a concentrations (Fig. 11).
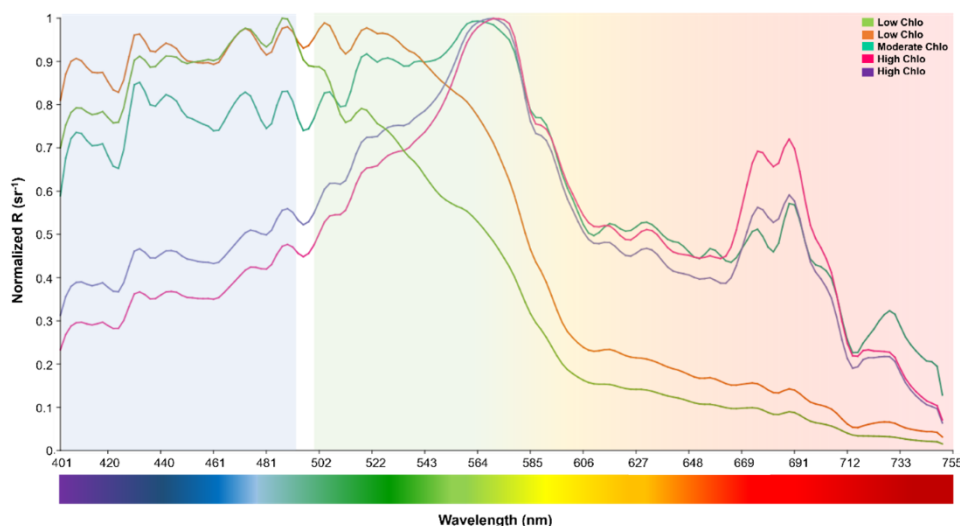
Figure 11: Microphytoplankton spectral signals at different Chlorophyll-a concentrations. Low chlorophyll-*a* (< 2 µg L⁻¹) (jasmine green and orange), moderate chlorophyll-a (> 4 to 7.9 µg L⁻¹) (aqua green), and high chlorophyll-a over 8 µg L⁻¹ (pink and purple).

320   Significant differences ($p < 0.01$) in spectra signals were detected at Ilque, with *Rhizosolenia* dominant, between January (low Chl-*a*= 0.8 µg L⁻¹) and March (high Chl-*a*= 1.6 µg L⁻¹). Also, in January, Pulelo (low Chl-*a*= 2.92 µg L⁻¹) and Isla Tenglo (high Chl-*a*= 5.93 µg L⁻¹) exhibited significant differences ($p < 0.01$) with a *Pseudo-nitzschia* dominant.

Regardless of the dominant species, at low Chl-*a* concentrations (< 2 µg L⁻¹), reflectance spectral signals exhibited more significant variability in the green-red bands (from 500 to 750 nm), while under moderate (> 4 µg L⁻¹) to high (> 8 µg L⁻¹)

325   Chl-*a* concentrations this variability was greater in the blue bands (~ 400-490 nm) (Fig. 11).

4 Discussion

4.1 Phytoplankton assemblages and spectral R(λ) variability

Currently, there are few datasets or studies that include in situ hyperspectral reflectance (R(λ)) as a new approach for studying phytoplankton (Casey et al., 2020). Through this study, a hyperspectral R(λ) data set, under variable oceanographic conditions,

330   was created with a total of 20 R(λ) spectra, aiming to characterise the fingerprint of phytoplankton corresponding to the typical

dominant species and total phytoplankton biomass concentrations in the study area (Iriarte et al., 2007; Alves-de-Souza et al., 2008; Jacob et al., 2014; Cuevas et al., 2019) under non-bloom conditions, except for the *Heterocapsa triquetra*.

The results reveal clear differences between the spectral signals of diatoms and dinoflagellates in both shape and magnitude. These differences are especially observed at the blue (~ 400-490 nm) and red to near infra-red bands (~ 650-740 nm), where

335 the absorption and fluorescence of accessory pigments are highest (Kramer et al., 2022). From a hierarchical cluster analysis (HCA) of the measured reflectance, two main groups (diatoms and dinoflagellates) and three sub-groups of phytoplankton assemblages were identified using the R(λ) spectrum, exhibiting variability not only between groups but also among genera. Although the R(λ) spectrum from different diatom genera was quite similar in shape and magnitude across the blue to green bands (~ 400-520 nm), the spectral signal allowed us to distinguish the "fingerprints" of different genera.

340 The pigments concentrations and community composition of phytoplankton and their effects on the reflectance spectrum have been demonstrated to be essential factors in developing optical fingerprints at the genera or species levels (Mao et al., 2010; Kramer et al., 2022; Gernez et al., 2023). Although increases in absorption and decreases in reflectance are generally correlated directly with changes in algal density (cell concentration) in monospecific laboratory experiments (Gitelson et al., 1999), a non-significant difference in spectral signals under different cell concentrations was detected in our field monitoring. This lack

345 of relationship between cell density and reflectance is probably seen in the range of densities observed in this study, which varied from 1,582,600 to 3,400 cells L^{-1}. In this context, the main factor affecting reflectance signals with differences in the shape of the curve for the same species was pigment concentration (Chl-*a*).

Recent studies have described a co-variation between pigments, both accessory and specific groups, and optical properties such as fluorescence, scattering or cellular grouping (Kramer et al., 2022). In this study, total Chl-*a* has been shown to play a

350 key role in the spectra with the R(λ) signal classification. The HCA applied clusters together assemblages corresponding to the same phytoplankton groups and genera detected under variable oceanographic conditions (mainly salinity and Chl-*a*) gathering locations under similar total biomass concentration (Chl-*a*) and phytoplankton community composition.

Open water circulation locations under different dominant diatoms genera, characterised by low total biomass concentrations (min. < 1 µg L^{-1}), higher salinity and the presence of dinoflagellates (*Gyrodinium* sp. and tecate dinoflagellates) were grouped

355 closer (Yaotal, Ilque and Pulelo). While stations with high Chl-*a* concentrations (min. >1 µg L^{-1}), located mainly in enclosed areas like Chaparano and Canal Tenglo, were part of another group. Further, it must be pointed out that locations with the lowest Chl-*a* concentrations also displayed the lowest mean values of abundance, making it difficult to establish the role of phytoplankton pigments and cell concentration (density) in the R(λ) signal registered.

Biological factors such as community composition and pigment concentrations have been demonstrated to be determining

360 factors to consider when studying reflectance signals. Even when measuring just Chl-*a* as a pigment, significant differences in

major spectral bands were observed based on this pigment concentration. In summer, under low Chl-*a* concentrations, peaks in reflectance in the green-red bands (~ 500-750 nm) exhibited significant variability. While spectral signals registered in autumn, under a more diverse community and higher Chl-*a* concentrations, displayed more variability in the blue bands (~ 400-490 nm). Therefore, variations in the blue bands (400-450 nm) are driven by the species composition under low Chl-*a* concentrations, in contrast to the green bands (500-550 nm) (Mao et al., 2010).

However, variability in reflectance can be associated with many factors, from biological (community composition, cellular morphology, cell density, pigments composition and concentration or physiological status) to physical-chemical (suspended matter, stratification, the roughness of the surface or the specular reflection) and/or even meteorological (wind speed, solar radiation, cloudiness, or solar angle) (Gitelson et al., 1999; Kim et al., 2016; Flores et al., 2022; Muñoz et al., 2023). It has to be considered that not only chlorophyll-a interacts with solar radiance, therefore affecting absorption/reflectance spectra, but also non-biological particles (CDOM & TSM), especially in coastal and estuarine optically complex waters (Gitelson et al., 1999; Mao et al., 2010; Kim et al., 2016; Flores et al., 2022; Kramer et al., 2022; Gernez et al., 2023; Muñoz et al., 2023). Also, variations in bio-optical water properties have been related not just to a punctual biological or non-biological parameter but to their interactions and seasonality (Simis et al., 2017; Flores et al., 2022; Adhikari et al., 2023; Muñoz et al., 2023). At the Baltic Sea, changes at the seasonal scale on phytoplankton succession (biological) and stratification (non-biological) in the water column have been associated with the optical signal (Simis et al., 2017).

Stratification plays a key role in vertical distribution of phytoplankton and matter at estuarine and coastal waters, where river and glacier melting discharges constitute an important input of CDOM and TSM which alters the bio-optical signal, especially at blue bands (Simis et al., 2017; Flores et al., 2022; Kramer et al., 2022; Adhikari et al., 2023; Muñoz et al., 2023). In the Patagonian Fjords, and especially within the Chiloé Inner Sea, high synchrony between Chl-*a* and turbid river plumes has been detected using remote sensing reflectance (Rrs$_{645}$ product) at 645 nm (Muñoz et al., 2023). Thus, distinguishing the effect of different factors on in situ reflectance signals is quite complex since that could be a nonlinear relationship. An essential factor, non-deal with this study, is the role of non-biological particles in the optical signal. Therefore, further research is necessary to understand the biological, i.e. phytoplankton composition and pigment concentration, including accessory pigments, and non-biological particles on the reflectance signal.

4.2 New technologies: limitations, opportunities and challenges

Optical technologies, like satellites, for phytoplankton remote detection, have been employed for decades (Hu et al., 2005; Alvain et al., 2008; Brewin et al., 2011; Shen et al., 2012; Moisan et al., 2017; Gernez et al., 2023). Although limitations in satellite observations associated with spatial-temporal and spectral bands resolution are well known (Muller-Karger et al., 2018; Schaeffer and Myer, 2020), new satellites using multi- or hyperspectral sensors like PACE and HICO have shown improvements in spatial (~ 1200-90 m) and/or spectral resolution (~ 350-900 nm) (Kramer et al., 2022; Gernez et al., 2023)

favouring the observation in the UV, visible and near-infrared bands. However, limitations remain associated with the number of spectral bands and the satellite orbit cycle, or they are caused by cloud cover and sun glint in remote areas.

Accurate observations represent a challenge in coastal areas where phytoplankton spatial-temporal variability changes rapidly.
395 The recent development of new technologies, like UAV and hyperspectral cameras, to detect and monitor phytoplankton blooms, focusing on harmful algae species at a high spatial-temporal resolution, can fill in the gaps of satellite data and also be able to validate satellite data with in situ measurements.

The usefulness of this technology in in situ measurements has been demonstrated, especially in coastal areas with current or future economic activities (Zhao and Ghedira, 2014). Thus, the optical system chosen for the spectral signal capture is an
400 essential factor. Currently, there are multiple possibilities, i.e., radiometers, hyperspectral and multispectral cameras, which offer different characteristics such as spectral resolutions, sizes and imaging systems (Kislik et al., 2018; Olivetti et al., 2023). Although hyperspectral cameras represent a high-cost technology nowadays, the high resolution of these cameras is considered the best option for phytoplankton and HAB monitoring in complex and small coastal areas with aquaculture activities such as fjords, bays and estuaries (Olivetti et al., 2023).

405 This study identified a series of advantages and challenges with using UAV and hyperspectral technology for detecting and identifying phytoplankton assemblages in complex coastal waters. One of the first advantages is the continuous spectral resolution that a hyperspectral camera provides, measuring each ~ 2 nm from 400 to 1000 nm approx., in comparison to multisensor cameras and satellites available, a powerful tool for differentiating between phytoplankton assemblages through changes in spectral signals at high resolution.

410 In our study area, a coastal system with a complex topography and high cloud cover throughout the year, capturing an effective satellite reflectance signal is a major challenge, especially on the same day and hour when water samples are being taken. Therefore, using a UAV for in situ reflectance measurement when a bloom has been declared is another advantage, with the possibility of monitoring at optimal altitudes (< 100 m) under cloud cover or other atmospheric factors such as suspended dust and other particles. Also, it must be mentioned that non high-qualified personnel are needed to drive the UAV.

415 However, UAV phytoplankton monitoring in remote areas is still a challenge. Although this technology could shorten sampling times, the dependency on a good network signal in the area constitutes a major limitation, particularly in remote areas where the network signal is easily lost. Also, weather conditions such as wind speed or precipitation, as previously identified (Kislik et al., 2018), can compromise the ability to fly, limiting the use of a UAV to monitor phytoplankton and HAB. Other limitations that appeared frequently during the study were related to technical aspects such as the flight time (batteries), the area coverage
420 limited by network signal and batteries durability, or the lack of reference points in a continuous body water (Kislik et al., 2018; Wu et al., 2019).

Two other important barriers which make it difficult to identify phytoplankton using reflectance data are the analysis of the vertical distribution of phytoplankton in the water column (~ 1-40 m) in both satellites and UAV systems, especially in the design of future algorithms; and the lack of a robust hyperspectral images library. Although recent works have included hyperspectral data for the study of phytoplankton assemblages, these datasets are still limited to specific areas and unavailable.

The high resolution of this new technology should allow us to improve the classical detection algorithms based on reflectance and/or absorbance ratios employed until now using satellite data (Mao et al., 2010; Tao et al., 2013; Gernez et al., 2023). The reflectance data registered in this study, together with information on oceanographic conditions and phytoplankton pigments and associated genera fingerprints, can be employed in the next step for the development of an accurate algorithm through machine learning not just to identify and differentiate phytoplankton genera blooms but also non-biological particles (suspended materials, sediments, etc.) and water characteristics. Therefore, future observations must combine UAV and next-generation satellite hyperspectral data with in situ biological (phytoplankton concentration, pigments, and taxonomy) and non-biological data (CDOM & TSM) collected at multiple and diverse environments.

5 Conclusions

This study aimed to take the first steps in identifying phytoplankton from in situ hyperspectral signals using UAV technology in a complex coastal system such as the Patagonian Fjords. Our results show the potential of hyperspectral data for detection and identification of phytoplankton assemblages providing evidence of differences between the spectral signals of diatoms (e.g., *Rhizosolenia* sp., *Pseudo-nitzschia* sp., and *Leptocylindrus* sp.) detected in the blue band (~ 400-490 nm) with those of dinoflagellates (e.g., *Heterocapsa triquetra*) observed in the red to near-red bands (~ 650-740 nm), regardless cellular concentration. Additionally, pigment concentrations have been validated as determinants, with Chl-*a* playing a significant role in classifying the reflectance spectra signal. Our study illustrates the great potential of hyperspectral technology and the usefulness of UAV systems to support and improve both satellite and in situ monitoring in complex coastal waters to advance ecological knowledge and environmental management. Thus, the hyperspectral sensor coupled to a UAV in remote areas could fill the satellite data gaps resulting from high cloud cover and extreme environmental conditions typical in the Patagonian Fjords. Finally, future analysis focusing on the impacts of varying water conditions and physical-chemical characteristics on the optical properties of the water and the reflectance spectrum (R(λ)) together with accessory cellular pigments need to be undertaken.

6 Data Availability Statement

The datasets for this study can be found in the https://hyops.ulagos.cl/app/inicio or by request from the corresponding authors

7 Author Contributions

Conceptualisation, PA and DV; methodology, PA and DP; validation, DV, IP and DP; formal analysis, PA and DP; investigation, PA, DP and CV; resources, DV; data curation, PA and DP; writing-original draft preparation, PA; writing-review and editing, DV, IP, DP, CV and PA; visualisation, PA and CV; supervision, DV; project administration, DV; funding acquisition, DV. All authors have read and agreed to the published version of the manuscript.

8 Competing interests

The authors declare that they have no conflict of interest.

9 Acknowledgements

We thank Ocean Data View, PRIMER and PAST software's for the data analysis and the construction of figures in the manuscript. Also, we thank Pamela Urrutia from MOWI, Cristobal Valdivieso and Lixandro Cisternas from ADENTU Igeniería SpA, and Constanza Obando and Elson Stuard for UAV training, technical and adequacy, and Dr Mattew Lee for meticulous review of the manuscript.

10 Financial support

This research was funded by FONDEF ID20I10369 and ID24I10271.

References

Adhikari, A., Menon, H.B., and Lotliker, A.: Coupling of hydrography and bio-optical constituents in a shallow optically complex region using ten years of in-situ data, ISPRS J. Photogramm., 202, 499-511, https://doi.org/10.1016/j.isprsjprs.2023.07.014, 2023.

Alvain, S., Moulin, C., Dandonneau, Y., and Loisel, H.: Seasonal distribution and succession of dominant phytoplankton groups in the global ocean: A satellite view, Global Biogeochem. Cycles., 22:GB3001, https://doi.org/10.1029/2007GB003154, 2008.

Alves-de-Souza, C., González, M.T., and Iriarte, J.L.: Functional groups in marine phytoplankton assemblages dominated by diatoms in fjords of southern Chile, J. Plankton Res., 30, 1233-1243, https://doi.org/10.1093/plankt/fbn079, 2008.

Anderson, D.: HABs in a changing world: a perspective on harmful algal blooms, their impacts, and research and management in a dynamic era of climactic and environmental change, Harmful Algae, 3:17, 2012.

475 Berdalet, E., Fleming, L.E., Gowen, R., Davidson, K., Hess, P., Backer, L.C., Moore, S.K., Hoagland, P., and Enevoldsen, H.: Marine harmful algal blooms, human health and wellbeing: challenges and opportunities in the 21st century, J. Mar. Biol. Assoc. U. K., 96(1), 61-91, https://doi.org/10.1017/S0025315415001733, 2016.

Brewin, R.J.W., Hardman-Mountford, N.J., Lavender, S.J., Raitsos, D.E., Hirata, T., Uitz J., Devred, E., Bricaud, A., Ciotti, A., and Gentili, B.: An intercomparison of bio-optical techniques for detecting dominant phytoplankton size class from satellite

480 remote sensing, Remote Sens. Environ., 115, 325-339, https://doi.org/10.1016/j.rse.2010.09.004, 2011.

Casey, K.A., Rousseaux, C.S., Gregg, W.W., Boss, E., Chase, A.P., Craig, S.E., Mouw, C.B., Reynolds, R.A., Stramski, D., Ackleson, S.G., Bricaud, A., Schaeffer, B., Lewis, M.R., and Maritorena, S.: A global compilation of in situ aquatic high spectral resolution inherent and apparent optical property data for remote sensing applications, Earth Syst. Sci. Data, 12, 1123-1139, https://doi.org/10.5194/essd-12-1123-2020, 2020.

485 Castillo, M.I., Cifuentes, U., Pizarro, O., Djurfeldt, L., and Caceres, M.: Seasonal hydrography and surface outflow in a fjord with a Deep sill: the Reloncaví fjord, Chile, Ocean Sci., 12, 533-544, https://doi.org/10.5194/os-12-533-2016, 2016.

Clarke, K.R., and Gorley, R.N.: PRIMER v7: User Manual/Tutorial, PRIMER-E Plymouth, 2015.

Cuevas, L.A., Tapia, F.J., Iriarte, J.L., González, H.E., Silva, N., and Vargas, C.A.: Interplay between freshwater discharge and oceanic waters modulates phytoplankton size-structure in fjords and channel systems of the Chilean Patagonia, Prog.

490 Oceanogr., 173, 103-113, https://doi.org/10.1016/j.pocean.2019.02.012, 2019.

Dávila, P.M., Figueroa, D., and Müller, E.: Freshwater input into the coastal ocean and its relation with the salinity distribution off austral Chile (35–55°S), Cont. Shelf Res., 22, 521-534, 2002.

Díaz, P.A., Álvarez, G., Varela, D., Pérez-Santos, I., Díaz, M., Molinet, C., Seguel, M., Aguilera-Belmonte, A., Guzman, L., Uribe, E., Rengel., J., Hernández, C., Segura, C., and Figueroa, R.I.: Impacts of harmful algal blooms on the aquaculture

495 industry: Chile as a case study, Perspectives in Phycol., 6(1-2), 39-50, https://doi.org/10.1127/pip/2019/0081, 2019.

Flores, R.P., Lara, C., Saldías, G.S., Vásquez, S.I., and Roco, A.: Spatio-temporal variability of turbid freshwater plumes in the Inner Sea of Chiloé, northern Patagonia, J. Mar. Syst., 228, 103709, https://doi.org/10.1016/j.jmarsys.2022.103709, 2022.

Gallagher, N.B.: Savitzky-Golay smoothing and differentiation filter, Eigenvector Research Inc., www.eigenvector.com. https://doi.org/10.13140/RG.2.2.20339.50725, 2020.

500 Garreaud, R., Lopez, P., Minvielle, M., and Rojas, M.: Large-Scale Control on the Patagonian Climate, J. Clim., 26, 215-230, https://doi.org/10.1175/JCLI-D-12-00001.1, 2013.

Gernez, P., Zoffoli, M.L., Lacour, T., Hernández Fariñas, T., Navarro, G., Caballero, I., and Harmel, T.: The many shades of red tides: Sentinel-2 optical types of highly-concentrated harmful algal blooms, Remote Sens. Environ., 287, 113486, https://doi.org/10.1016/j.rse.2023.113486, 2023.

505 Gitelson, A.A., Schalles, J.F., Rundquist, D.C., Schiebe, F.R., and Yacobi, Y.Z.: Comparative reflectance properties of algal cultures with manipulated densities, J. Appl. Phycol., 11, 345-354, 1999.

Glibert, P.M.: Harmful algae at the complex nexus of eutrophication and climate change, Harmful Algae, 91, 101583, https://doi.org/10.1016/j.hal.2019.03.001, 2020.

Gobler, C.J.: Climate Change and Harmful Algal Blooms: Insights and perspective, Harmful Algae, 91, https://doi.org/10.1016/j.hal.2019.101731, 2020.

González, H.E., Nimptsch, J., Giesecke, R., and Silva, N.; Organic matter distribution, composition and its possible fate in the Chilean North-Patagonian estuarine system, Sci. Total Environ., 657, 1419-1431, https://doi.org/10.1016/j.scitotenv.2018.11.445, 2019.

Hammer, Ø., Harper, D.A.T., and Ryan, P.D.: PAST: Paleontological Statistics Software Package for Education and Data Analysis, Palaeontologia Electronica, 4(1), 1-9, 2001.

Heisler, J., Glibert, P.M., Burkholder, J.M., Anderson, D.M., Cochlan, W., Dennison, W.C., Dortch, Q., Gobler, C.J., Heil, C.A., Humphries, E., Lewitus, A., Magnien, R., Marchall, H.G., Sellner, K., Stockwell, D.A., Stoecker, D.K., and Suddleson, M.: Eutrophication and harmful algal blooms: A scientific consensus, Harmful Algae, 8, 3-13, https://doi.org/10.1016/j.hal.2008.08.006, 2008.

Henson, S.A., Cael, B.B., Allen, S.R., and Dutkiewicz, S.: Future phytoplankton diversity in a changing climate, Nat. Commun., 12, 5372, https://doi.org/10.1038/s41467-021-25699-w, 2021.

Hong, S.M., Baek, S-S., Yun, D., Kwon, Y-H., Duan, H., Pyo J., and Cho K.H.: Monitoring the vertical distribution of HABs using hyperspectral imagery and deep learning models, Sci. Total Environ., 794, 148592, https://doi.org/10.1016/j.scitotenv.2021.148592, 2021.

Hu, C., Muller-Karger, F.E., Taylor, C.J., Carder, K.L., Kelble, C., Johns, E., and Heil, C.A.: Red tide detection and tracing using MODIS fluorescence data: A regional example in SW Florida coastal waters, Remote Sens. Environ., 97, 311-321, https://doi.org/10.1016/j.rse.2005.05.013, 2005.

Iriarte, J.L., González, H.E., Liu, K.K., Rivas, C., and Valenzuela, C.: Spatial and temporal variability of chlorophyll and primary productivity in surface waters of southern Chile (41.5-43°S), Estuarine, Coastal Shelf Sci., 74, 471-480, https://doi.org/10.1016/j.ecss.2007.05.015, 2007.

Jacob, B.G., Tapia, F.J., Daneri, G., Iriarte, J.L., Montero, P., Sobarzo, M., and Quiñones, R.A.: Springtime size-fractionated primary production across hydrographic and PAR-light gradients in Chilean Patagonia (41–50°S), Prog. Oceanogr., 129, 75-84, https://doi.org/10.1016/j.pocean.2014.08.003, 2014.

Jeffrey, S.W., and Vesk, M.: Introduction to marine phytoplankton and their pigment signatures, in: Phytoplankton Pigments in Oceanography: Guidelines to Modern Methods, edited by: Jeffrey, S.W., Mantoura, R.F.C., and Wright, S.W., UNESCO Publ., Paris, France, 37-84, 1997.

Kim, H.M., Yoon, H.J., Jang, S.W., Kwak, S.N., Sohn, B.Y., Kim, S.G., and Kim, D.H.: Application of Unmanned Aerial Vehicle Imagery for Algal Bloom Monitoring in River Basin, Int. J. Control Autom., 9, 203-220, 2016.

Kimura, F., Morinaga, A., Fukushima, M., Ishiguro, T., Sato, Y., Sakaguchi, A., Kawashita, T., Yamamoto, I., and Kobayashi,
540 T.: Early Detection System of Harmful Algal Bloom Using Drones and Water Sample Image Recognition, Sens. Mater.,
31(12), 4155-4171, https://doi.org/10.18494/SAM.2019.2417, 2019.

Kislik, C., Dronova, I., and Kelly, M.: UAVs in Support of Algal Bloom Research: A Review of Current Applications and
Future Opportunities, Drones, 2:35, https://doi.org/10.3390/drones2040035, 2018.

Kramer, S.J., Siegel, D.A., Maritorena, S., and Catlett, D.: Modeling surface ocean phytoplankton pigments from hyperspectral
545 remote sensing reflectance on global scales, Remote Sens. Environ., 270-112879, https://doi.org/10.1016/j.rse.2021.112879,
2022.

Legendre, L.: The significance of microalgal blooms for fisheries and for the export of particulate organic carbon in oceans, J.
Plankton Res.,12(4),681-699, 1990.

León-Muñoz, J., Urbina, M.A., Garreaud, R., and Iriarte, J.L.: Hydroclimatic conditions trigger record harmful algal bloom in
550 western Patagonia (summer 2016), Nature Sci. Rep., 8, 1330, https://doi.org/10.1038/s41598-018-19461-4, 2018.

Le Quéré, C., Harrison, S.P., Prentice, C., Buitenhuis, E.T., Aumont, O., Bopp L., Claustre, H., Cotrim Da Cunha, L., Geider,
R., Giraud, X., Klaas, C., Kohfeld, K.E., Legendre, L., Manizza, M., Platt, T., Rivkin, R.B., Sathyendranath, S., Uitz, J.,
Watson, A.J., and Wolf-Gladrow, D.: Ecosystem dynamics based on plankton functional types for global ocean
biogeochemistry models, Global Change Biol., 11, 2016-2040, https://doi.org/10.1111/j.1365-2486.2005.01004.x, 2005.

555 Li, Y., Zhou, Q., Zhang, Y., Li, J., and Shi, K.: Research Trends in the Remote Sensing of Phytoplankton Blooms: Results
from Bibliometrics, Remote Sens., 13, 4414, https://doi.org/10.3390/rs13214414, 2021.

Lincoqueo, S.L.: Catálogo de microalgas marinas, nocivas para salmónidos. Archipiélago de Chiloé, Kimeltuán SpA., 2019.

Linford, P., Pérez-Santos, I., Montero, P., Díaz, P.A., Aracena, C., Pinilla, E., Barrera, F., Castillo, M., Alvera-Azcárate, A.,
Alvarado, M., Soto, G., Pujol, C., Schwerter, C., Arenas-Uribe, S., Navarro, P., Mancilla-Gutiérrez, G., Altamirano, R., San
560 Martín, J., and Soto-Riquelme, C.: Oceanographic processes driving low-oxygen conditions inside Patagonian fjords,
Biogeosciences, 21, 1433-1459, https://doi.org/10.5194/bg-21-1433-2024, 2024.

Mao, Z., Stuart, V., Pan, D., Chen, J., Gong, F., Huang, H., and Zhu, Q.: Effects of phytoplankton species composition on
absorption spectra and modelled hyperspectral reflectance, Ecol. Inform., 5, 359-366,
https://doi.org/10.1016/j.ecoinf.2010.04.004, 2010.

565 Mardones, J.I., and Clément, A.: Manual de microalgas del sur de Chile, Plancton Andino SpA., Puerto Varas, 186 pp., 2016.

McEliece, R., Hinz, S., Guarini, J.M., and Coston-Guarini, J.: Evaluation of Nearshore and Offshore Water Quality Assessment
Using UAV Multispectral Imagery, Remote Sens., 12, 2258, https://doi.org/10.3390/rs12142258, 2020.

Merkens, J.L., Reimann, L., Hinkel, J., and Vafeidis, A.T.: Gridded population projections for the coastal zone under the
Shared Socioeconomic Pathways, Glob. Planet. Change., 145, 57-66, https://doi.org/10.1016/j.gloplacha.2016.08.009, 2016.

570   Min, J.E., Lee, S.K., and Ryu, J.H.: Advanced surface-reflected radiance correction for airborne hyperspectral imagery in coastal red tide detection, ISPRS Ann. Photogramm. Remote Sens. Spatial Inf. Sci., 3, 73-80, https://doi.org/10.5194/isprs-annals-V-3-2021-73-2021, 2021.

Moisan, T.A., Rufty, K.M., Moisan, J.R., and Linkswiler, M.A.: Satellite Observations of Phytoplankton Functional Type Spatial Distributions, Phenology, Diversity, and Ecotones, Front. Mar. Sci., 4, 189, https://doi.org/10.3389/fmars.2017.00189,
575   2017.

Moses, W.J., Gitelson, A.A., Perk, R.L., Gurlin, D., Rundquist, D.C., Leavitt, B.C., Barrow, T.M., and Brakhage, P.: Estimation of chlorophyll-a concentration in turbid productive waters using airborne hyperspectral data, Water Res., 46, 993-1004, https://doi.org/10.1016/j.watres.2011.11.068, 2012.

Muller-Karger, F.E., Hestir, E., Ade, C., Turpie, K., Roberts, D.A., Siegel, D., Miller, R.J., Humm, D., Izenberg, N., Keller,
580   M., Morgan, F., Frouin, R., Dekker, A.G., Gardner, R., Goodman, J., Schaeffer, B., Franz, B.A., Pahlevan, N., Mannino, A.G., Concha, J.A., Ackleson, S.G., Cavanaugh, K.C., Romanou, A., Tzortziou, M., Boss, E.S., Pavlick, R., Freeman, A., Rousseaux, c.S., Dunne, J., Long, M.C., Klein, E., McKinley, G.A., Goes, J., Letelier, R., Kavanaugh, M., Roffer, M., bracher, A., Arrigo, K.R., Dierssen, H., Zhang, X., Davis, F.W., Best, B., Guralnick, R., Moisan, J., Sosik, H.M., Kudela, R., Mouw, C.B., Barnard, A.H., Palacios, S., Roesler, C., Drakou, E.G., Appeltans, W., and Jetz, W.: Satellite sensor requirements for monitoring
585   essential biodiversity variables of coastal ecosystems, Ecol. Appl., 28(3), 749-760, https://doi.org/10.1002/eap.1682, 2018.

Muñoz, R., Lara, C., Arteaga, J., Vásquez, S.I., Saldías, G.S., Flores, R.P., He, J., Broitman, B.R., and Cazelles, B.: Temporal Synchrony in Satellite-Derived Ocean Parameters in the Inner Sea of Chiloé, Northern Patagonia, Chile, Remote Sens., 15, 2182, https://doi.org/10.3390/rs15082182, 2023.

Neumann, B., Vafeidis, A.T., Zimmermann, J., and Nicholls, R.J.: Future Coastal Population Growth and Exposure to Sea-
590   Level Rise and Coastal Flooding - A Global Assessment, PLoS ONE, 10(3):e0118571, https://doi.org/10.1371/journal.pone.0118571, 2015.

Olivetti, D., Cicerelli, R., Martinez, J-M., Almeida, T., Casari, R., Borges, H., and Roig, H.: Comparing Unmanned Aerial Multispectral and Hyperspectral Imagery for Harmful Algal Bloom Monitoring in Artificial Ponds Used for Fish Farming, Drones, 7:410, https://doi.org/10.3390/drones7070410, 2023.

595   Pérez-Santos, I., Garcés-Vargas, J., Schneider, W., Ross, L., Parra, S., and Valle-Levinson, A.: Double-diffusive layering and mixing in Patagonian fjords, Prog. Oceanogr., 129, 35-49, https://doi.org/10.1016/j.pocean.2014.03.012, 2014.

Ruffin, C., and King, R.L.: The analysis of hyperspectral data using Savitzky-Golay filtering-theoretical basis, IEEE International Geoscience and Remote Sensing Symposium 1999 (IGARSS'99), 2, 756-758, https://doi.org/10.1109/IGARSS.1999.774430, 1999.

600   Saldías, G.S., Sobarzo, M., and Quiñones, R.: Freshwater structure and its seasonal variability off western Patagonia, Prog. Oceanogr., 174, 143-153, https://doi.org/10.1016/j.pocean.2018.10.014, 2019.

Schaeffer, B.A., and Myer, M.H.: Resolvable estuaries for satellite derived water quality within the continental United States, Remote Sens. Lett., 11(6), 535-544, https://doi.org/10.1080/2150704X.2020.1717013, 2020.

Schlitzer, R.: Ocean Data View 2023, https://odv.awi.de.

605 Shen, Li., Xu, H., and Guo, X.: Satellite Remote Sensing of Harmful Algal Blooms (HABs) and a Potential Synthesized Framework, Sensors, 12, 7778-7803, https://doi.org/10.3390/s120607778, 2012.

Silva, N., Vargas, C.A., and Prego, R.: Land-ocean distribution of allochthonous organic matter in surface sediments of the Chiloé and Aysén interior seas (Chilean Northern Patagonia), Cont. Shelf Res., 31, 330-339, https://doi.org/10.1016/j.csr.2010.09.009, 2011.

610 Silva, N., and Vargas, C.A.: Hypoxia in Chilean Patagonian Fjords, Prog. Oceanogr., 129, 62-74, https://doi.org/10.1016/j.pocean.2014.05.016, 2014.

Simis, S.G.H., Ylöstalo, P., Kallio, K.Y., Spilling, K., and Kutser, T.: Contrasting seasonality in optical biogeochemical properties of the Baltic Sea, PLoS ONE, 12(4):e0173357, https://doi.org/10.1371/journal.pone.0173357, 2017.

Soto, D., León-Muñoz, J., Dresdner, J., Luengo, C., Tapia, F.J., and Garreaud, R.: Salmon farming vulnerability to climate
615 change in southern Chile: understanding the biophysical, socioeconomic and governance links, Rev Aquac., 11, 354-374, https://doi.org/10.1111/raq.12336, 2019.

Soto, D., León-Muñoz, J., Garreaud, R., Quiñones, R.A., and Morey, F.: Scientific warnings could help to reduce farmed salmon mortality due to harmful algal blooms, Mar. Policy., 132, 104705, https://doi.org/10.1016/j.marpol.2021.104705, 2021.

Sournia, A.: Red-tide and toxic marine phytoplankton of the world ocean: an inquiry into biodiversity, in: Harmful marine
620 algal blooms: Proceedings of the Sixth International Conference on toxic marine phytoplankton, edited by: Lassus P., et al., Lavoisier, France, 103-112, 1995.

Szekielda, K.H., Marmorino, G.O., Maness, S.J., Donato, T., Bowles, J.H., Miller, W.D., and Rhea, W.J.: Airborne hyperspectral imaging of cyanobacteria accumulations in the Potomac River, J. Appl. Remote Sens., 1, 013544, https://doi.org/10.1117/1.2813574, 2007.

625 Tao, B., Mao, Z., Pan, D., Shen, Y., Zhu, Q., and Chen, J.: Influence of bio-optical parameter variability on the reflectance peak position in the red band of algal bloom waters, Ecol. Inform., 16, 17-24, https://doi.org/10.1016/j.ecoinf.2013.04.005, 2013.

Torres, R., Silva, N., Reid, R., and Frangopulos, M.: Silicic acid enrichment of subantarctic surface water from continental inputs along the Patagonian archipelago interior sea (41–56°S), Prog. Oceanogr., 129, 50-61,
630 https://doi.org/10.1016/j.pocean.2014.09.008, 2014.

Trainer, V.L., Moore, S.K., Hallegraeff, G., Kudela, R.M., Clement, A., Mardones, J.I., and Cochlan, W.P.: Pelagic harmful algal blooms and climate change: Lessons from nature's experiments with extremes, Harmful Algae, 91, 101591, https://doi.org/10.1016/j.hal.2019.03.009, 2020.

Troupin, C., Barth, A., Sirjacobs, D., Ouberdous, M., Brankart, J-M., Brasseur, P., Rixen, M., Alvera-Azcárate, A., Belounis, M., Capet, A., Lenartz, F., and Toussaint, M-E.: Generation of analysis and consistent error fields using the Data Interpolating Variational Analysis (Diva), Ocean Modelling, 52-53, 90-101, https://doi.org/10.1016/j.ocemod.2012.05.002, 2012.

Ugarte, A., Romero, J., Farías, L., Sapiains, R., Aparicio-Rizzo, P., Ramajo, L., Aguirre, C., Masotti, I., Jacques, M., Aldunce, P., Alonso, C., Azócar, G., Bada, R., Barrera, F., Billi, M., Boisier, J., Carbonell, P., De la Maza, L., De la Torre, M., Espinoza-González, O., Faúndez, J., Garreaud, R., Guevara, G., González, M., Guzmán, L., Ibáñez, J., Ibarra, C., Marín, A., Mitchell, R., Moraga, P., Narváez, D., O'Ryan, R., Pérez, C., Pilgrin, A., Pinilla, E., Rondanelli, R., Salinas, M., Sánchez, R., Sanzana, K., Segura, C., Valdebenito, P., Valenzuela, D., Vásquez, S., and Williamson, C.: «Marea roja» y cambio global: elementos para la construcción de una gobernanza integrada de las Floraciones de Algas Nocivas (FAN), Centro de Ciencia del Clima y la Resiliencia (CR)2, (ANID/FONDAP/15110009), 1-84, available on www.cr2.cl/fan, 2022.

Utermöhl, H.: Zur Vervollkommung der quantitativen Phytoplankton-Methodik. Mitteilungen Internationale Vereinigung für Theoretische und Angewandte Limnologie, 9, 1-38, 1985.

Valle-Levinson. A.: Contemporary Issues in Estuarine Physics, Cambridge University Press, New York, USA, 273-307, 2010.

Van der Merwe, D., and Price, K.P.: Harmful Algal Bloom Characterisation at Ultra-High Spatial and Temporal Resolution Using Small Unmanned Aircraft Systems, Toxins, 7, 1065-1078, https://doi.org/10.3390/toxins7041065, 2015.

Wu, D., Li, R., Zhang, F., and Liu, J.: A review on drone-based harmful algae blooms monitoring, Environ Monit. Assess., 191-211, https://doi.org/10.1007/s10661-019-7365-8, 2019.

Xie, H., Luo, X., Xu, X., Tong, X., Jin, Y., Pan, H., and Zhou, B.: New hyperspectral difference water index for the extraction of urban water bodies by the use of airborne hyperspectral images, J. Appl. Remote Sens., 8(1), 085098-085098, https://doi.org/10.1117/1.JRS.8.085098, 2014.

Zhao, J., and Ghedira, H.: Monitoring red tide with satellite imagery and numerical models: A case study in the Arabian Gulf, Mar. Pollut. Bull., 79, 305-313, https://doi.org/10.1016/j.marpolbul.2013.10.057, 2014.